Modeling Thermodynamic Ice-Ocean Interactions at the Base of an Ice Shelf

2 authors:

David M. Holland
New York University
179 PUBLICATIONS   **6,668** CITATIONS

SEE PROFILE

Adrian Jenkins
Northumbria University
194 PUBLICATIONS   **10,128** CITATIONS

SEE PROFILE

Some of the authors of this publication are also working on these related projects:

Project   Glacial landforms of the West Antarctic Shelf View project

Project   Center for Global Sea Level Change of NYU Abu Dhabi G1204 View project

Modeling Thermodynamic Ice–Ocean Interactions at the Base of an Ice Shelf

DAVID M. HOLLAND

Lamont-Doherty Earth Observatory, Palisades, New York

ADRIAN JENKINS

British Antarctic Survey, Cambridge, United Kingdom

ABSTRACT

Models of ocean circulation beneath ice shelves are driven primarily by the heat and freshwater fluxes that are associated with phase changes at the ice–ocean boundary. Their behavior is therefore closely linked to the mathematical description of the interaction between ice and ocean that is included in the code. An hierarchy of formulations that could be used to describe this interaction is presented. The main difference between them is the treatment of turbulent transfer within the oceanic boundary layer. The computed response to various levels of thermal driving and turbulent agitation in the mixed layer is discussed, as is the effect of various treatments of the conductive heat flux into the ice shelf. The performance of the different formulations that have been used in models of sub-ice-shelf circulation is assessed in comparison with observations of the turbulent heat flux beneath sea ice. Formulations that include an explicit parameterization of the oceanic boundary layer give results that lie within about 30% of observation. Formulations that use constant bulk transfer coefficients entail a definite assumption about the level of turbulence in the water column and give melt/freeze rates that vary by a factor of 5, implying very different forcing on the respective ocean models.

1. Introduction

The continental shelf seas surrounding Antarctica most frequently attract attention because they are the source regions of Antarctic Bottom Water. It is commonly assumed that atmospheric forcing of the ocean and ice cover is the primary driving mechanism behind the deep convection that occurs over the continental slope (e.g., Gill 1973). However, poleward of the shelf break, 40% of the sea surface is covered by floating ice shelves, which range in thickness from 100 to 2000 m and therefore completely isolate the ocean from the atmosphere. Circulation beneath the ice shelves and the associated meltwater input have a profound impact on shelf water properties (Foldvik et al. 1985; Jacobs et al. 1985; Fahrbach et al. 1994; Hellmer et al. 1999). Toggweiler and Samuels (1995) suggest that up to 75% of all the ocean's deep waters may retain a signature of this meltwater input.

The interaction between ice shelves and the ocean is thus a potentially important element of the climate system, and in recent years numerical models have been used to evaluate the key processes operating in sub-ice-shelf cavities (Williams et al. 1999). Upper boundary conditions derived from a thermodynamic model of the ice–ocean interaction have been applied to ocean models of varying sophistication. Dynamic models of the ice shelf itself have not been included, so the ice–ocean interface has been treated as a fixed boundary. The disparity of timescales between the slowly flowing ice shelf and the relatively fast flowing waters beneath provides some justification for this approach. Although the specification of the upper boundary conditions represents a computationally small and simple component of most sub-ice-shelf circulation models, it is of crucial importance. A correct estimate of the surfaces fluxes is essential to a realistic simulation of the sub-ice-shelf circulation and to the utility of the results for estimating the mass balance of the ice shelves.

In this paper we focus on the mathematical description of the ice–ocean interaction. We present an hierarchy of models describing the heat and freshwater exchange at and near the ice–ocean interface. Our aim is to compare the behavior of the differing upper boundary formulations that have been used in models of sub-ice-shelf circulation to date and to introduce a new formulation that closely follows the work of McPhee et al. (1987). For a related comparative study, but in the context of sea ice–ocean coupling, the reader is referred to

Corresponding author address: David M. Holland, Courant Institute of Mathematical Sciences, 251 Mercer St., Warren Weaver Hall, 907, New York University, MC 0711, New York, NY 10012.
E-mail: holland@cims.nyu.edu

work by Holland et al. (1997). We also compare the results of the various models with recent observations of heat flux in the turbulent boundary layer beneath sea ice.

The fundamental assumption in all the models is that phase changes occur in thermodynamic equilibrium so that the temperature and salinity at the ice–ocean interface are always related by an expression for the freezing point at the appropriate depth. The problem becomes one of calculating the heat and freshwater fluxes that result from deviations in the far-field ocean properties from freezing point conditions. Our treatments of the processes occurring in the oceanic boundary layer differ only in the sophistication with which turbulent diffusion of heat and salt is modeled. On the ice side of the interface the flow is laminar and only the diffusion of heat need be considered because salt cannot diffuse through the solid ice matrix. The problem is that diagnosis of the temperature gradient at the ice shelf base requires solution of the equation for heat advection and diffusion throughout the ice shelf. As the ice flow is unknown, we require a reduced form of this equation that is tractable but captures the essential features of the full solution.

In common with most models of sub-ice-shelf circulation, we consider all phase changes to occur at the ice–ocean boundary, regardless of whether the far-field ocean conditions are above or below freezing. We do not consider the process of frazil ice growth in supercooled parts of the water column, although observations and modeling (Oerter et al. 1992; Bombosch and Jenkins 1995) suggest that deposition of suspended ice crystals is the dominant mechanism of basal growth beneath ice shelves. Thus, while it is instructive to intercompare the response of the different boundary formulations to supercooling in the ocean, direct comparisons between models and observations are only valid for melting conditions. It is possible to treat the thermodynamics of frazil ice growth in a manner analogous to that outlined below for melting and freezing at a solid boundary, but the incorporation of frazil ice into an ocean model requires the addition of an ice conservation equation (Omstedt and Svensson 1984; Mellor et al. 1986; Jenkins and Bombosch 1995).

2. Thermodynamic models of ice–ocean interaction

The objective of modeling the ice–ocean interaction is to obtain as realistic as possible a melt rate at the ice-shelf base. We now define and solve the necessary equations to achieve this. The far-field quantities are the prescribed interior properties of the ice shelf and the properties of the upper layer or level of the ocean model. We are interested in determining the characteristics exactly at the ice–ocean interface where there are three physical constraints: the interface must be at the freezing point and both heat and salt must be conserved at the interface during any phase changes. This gives a system

of up to three equations in up to three unknowns, namely, the interface temperature, salinity, and melt rate.

To assist the discussion below, the relevant layers, temperatures, salinities, and heat and salt fluxes are shown schematically in Fig. 1. The ocean mixed layer has a temperature T_M and salinity S_M, which are not necessarily equal to the respective ice–ocean interface properties T_B and S_B. The gradients in temperature and salinity through the boundary layer drive heat and salt fluxes between the interface and the mixed layer. The temperature gradient in the ice at the base of the ice shelf drives a heat flux from the interface into the ice shelf, which has a surface temperature denoted by T_s and a bulk salinity denoted by S_I.

a. Fundamental equations

1) FREEZING POINT DEPENDENCE

The freezing point of seawater is a weakly nonlinear function of salinity and a linear function of pressure (Millero 1978). This relationship between temperature and salinity at the ice–ocean interface will be one of three equations that will have to be solved simultaneously, so it is simpler to work with a linearized version:

$$T_B = aS_B + b + cp_B, \qquad (1)$$

where p_B is the pressure at the interface. The values of the empirical constants a, b, and c are given in Table 1 along with other constants and parameters used in this study. The formula is valid only in the salinity range 4–40 psu and does not apply to pure freshwater.

2) HEAT CONSERVATION

At the ice–ocean interface, the divergence of the heat flux balances the sink or source of latent heat caused by melting or freezing:

$$Q_I^T - Q_M^T = Q_{\text{latent}}^T. \qquad (2)$$

The latent heat term is given by

$$Q_{\text{latent}}^T = -\rho_M w_B L_f, \qquad (3)$$

where $\rho_M w_B$ represents the mass of ice that is melted ($w_B > 0$) or frozen ($w_B < 0$) per unit time. The estimation of the diffusive heat fluxes is discussed in detail below.

3) SALT CONSERVATION

An equation analogous to (3) describes the salt flux required to maintain the boundary salinity at S_B in the presence of the "freshwater" flux associated with melting or freezing of ice having a salinity of S_I:

$$Q_{\text{brine}}^S = \rho_M w_B(S_I - S_B). \qquad (4)$$

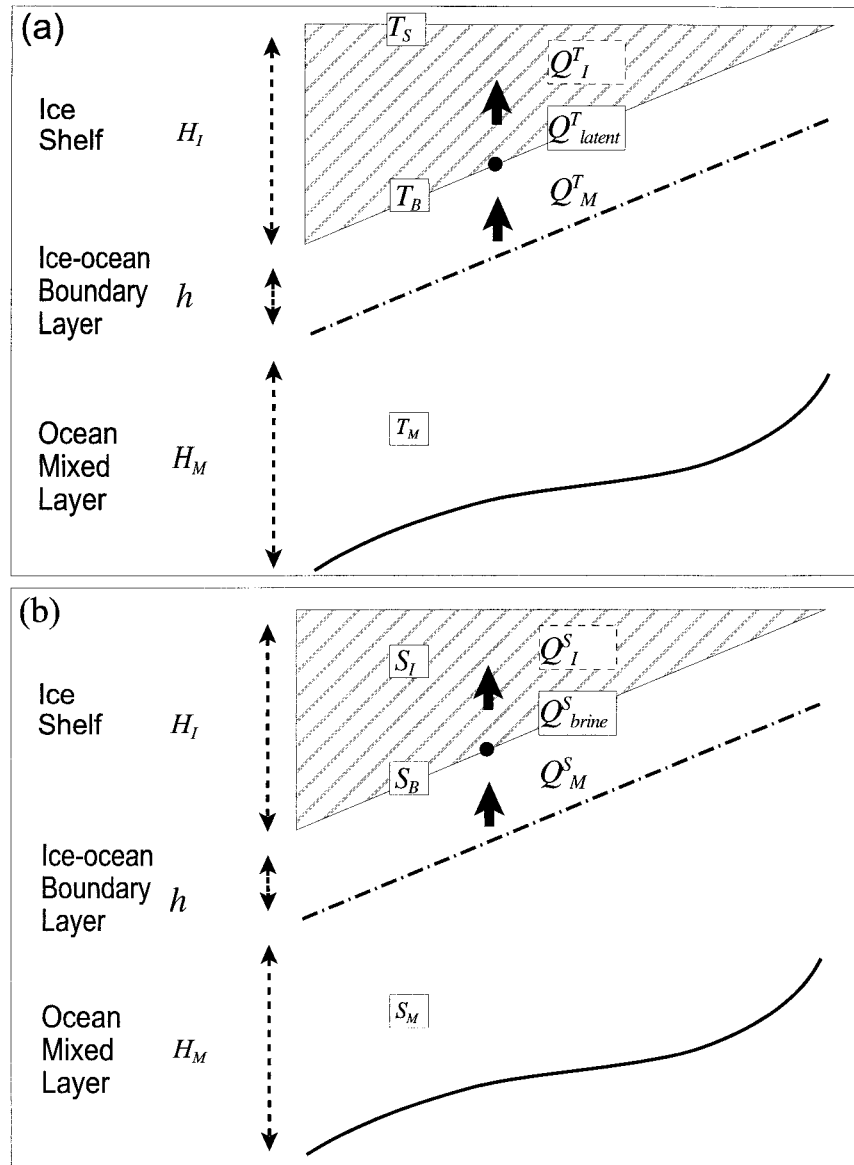This is balanced by the salt flux divergence at the interface:

FIG. 1. Schematic representation of (a) the heat and (b) the salt balance at the base of an ice shelf. The slope of the ice shelf base is greatly exaggerated for illustrative purposes.

$$Q_I^S - Q_M^S = Q_{\text{brine}}^S. \qquad (5)$$

The diffusive flux of salt into the ice shelf, Q_I^S, is identically zero and will be discussed no further, while the estimation of the diffusive flux through the oceanic boundary layer will be addressed below. Continental ice that melts from the base of an ice shelf has a salinity of zero, but when seawater freezes, brine is usually trapped within the forming ice, giving it a nonzero bulk salinity. Observations of marine ice found at the base of ice shelves with salinities of 0.025 psu (Eicken et al. 1994) indicate that a very effective desalination process must operate. As further evidence, additional observations (Oerter et al. 1992) show very low salinities of

approximately 0.100 and suggest that to a good approximation we can treat S_I as zero always.

b. Modeling the oceanic fluxes

1) A ONE-EQUATION FORMULATION

The simplest approach recognizes that whatever the details of heat and salt transfer through the oceanic boundary layer, the overall effect is to cause the upper layer of the ocean to relax toward the freezing point. If this relaxation is assumed to occur instantaneously, there is no distinction between interface and mixed layer properties, and the ice–ocean interaction can be de-

TABLE 1. Model parameters and constants.

Parameter	Symbol	Units	Value
Salinity coefficient of freezing equation	a	°C psu^{-1}	-5.73×10^{-2}
Constant coefficient of freezing equation	b	°C	9.39×10^{-2}
Bernoulli numbers	B_n	dimensionless	
Ocean surface buoyancy flux	B_M	m^2 s^{-2}	
Pressure coefficient of freezing equation	c	°C Pa^{-1}	-7.53×10^{-8}
Constants of integration	c_1, c_2	dimensionless	
Momentum exchange coefficient	c_d	dimensionless	1.50×10^{-3}
Specific heat capacity ice shelf	c_{pI}	J kg^{-1} K^{-1}	2009.0
Specific heat capacity mixed layer	c_{pM}	J kg^{-1} K^{-1}	3974.0
Coriolis parameter	f	s^{-1}	-1.00×10^{-4}
Gravitational acceleration	g	m s^{-2}	9.81
Thickness of boundary layer	h	m	
Thickness of viscous sublayer	h_ν	m	~ 0.001
Thickness of ice shelf	H_I	m	~ 1000
Thickness of mixed layer	H_M	m	~ 10
Von Kármán's constant	k	dimensionless	0.40
Latent heat fusion	L_f	J kg^{-1}	3.34×10^5
Obukhov length	L_o	m	
Solutions of characteristic polynomial	m, m_1, m_2	dimensionless	
Nusselt number	Nu	dimensionless	$\gg 1$
Pressure at ice shelf base	p_B	Pa	$\sim 1.0 \times 10^7$
Prandtl number	Pr	dimensionless	13.8
Conductive heat flux through ice shelf	Q_I^T	W m^{-2}	
Latent heat at ice–ocean interface	Q_{latent}^T	W m^{-2}	
Diffusive heat flux in boundary layer	Q_M^T	W m^{-2}	
Diffusive salt flux through ice shelf	Q_I^S	psu m^{-1} s^{-1}	
Salt flux at ice–ocean interface	Q_{brine}^S	psu m^{-1} s^{-1}	
Diffusive salt flux in boundary layer	Q_M^S	psu m^{-1} s^{-1}	
Ratio of melt/freeze rates	r	dimensionless	
Critical flux Richardson number	R_c	dimensionless	0.20
Schmidt number	Sc	dimensionless	2432
Bulk salinity of ice shelf	S_I	psu	0
Salinity at ice–ocean interface	S_B	psu	Prognostic
Salinity of mixed layer	S_M	psu	~ 34.5
Time coordinate	t	s	
Temperature at ice shelf surface	T_S	°C	~ -25.0
Temperature at ice–ocean interface	T_B	°C	Prognostic
Temperature of mixed layer	T_M	°C	~ -1.85
Thermal driving	T_*	°C	
Ice shelf flow velocity	U_I	m s^{-1}	
Ocean mixed layer velocity	U_M	m s^{-1}	
Friction velocity ice–ocean	U_*	m s^{-1}	
Melt rate at ice shelf base	w_B	m s^{-1}	Prognostic
Vertical velocity of ice shelf	w_I	m s^{-1}	
Vertical geopotential coordinate	z	m	
Salinity contraction coefficient	β_S	psu^{-1}	
Thermal expansion coefficient	β_T	°C^{-1}	
Molecular thermal conductivity ice shelf	κ_I^T	m^2 s^{-1}	1.14×10^{-6}
Thermal diffusivity of mixed layer	κ_M^T		
Molecular salt conductivity ice shelf	κ_I^S	m^2 s^{-1}	0.0
Salt diffusivity mixed layer	κ_M^S	m^2 s^{-1}	
Ice shelf reference density	ρ_I	kg m^{-3}	920.0
Ocean reference density	ρ_M	kg m^{-3}	1025.0
Ratio of thermal driving to thermal forcing	Θ	dimensionless	
Thermal exchange velocity	γ_T	m s^{-1}	$\sim 1.00 \times 10^{-4}$
Salinity exchange velocity	γ_S	m s^{-1}	$\sim 5.05 \times 10^{-7}$
Kinematic viscosity of sea water	ν	m^2 s^{-1}	1.95×10^{-6}
Péclet number	Υ	dimensionless	
Temperature gradient amplification factor	Π	dimensionless	
Turbulent transfer parameter	Γ_{Turb}	dimensionless	
Thermal molecular transfer parameter	Γ_{Mole}^T	dimensionless	
Salinity molecular transfer parameter	Γ_{Mole}^S	dimensionless	
Stability parameter	η_*	dimensionless	≤ 1
Stability constant	ξ_N	dimensionless	0.052

scribed completely using Eq. (1). Such a formulation has been widely used in large-scale ocean–atmosphere–sea ice models (Holland 1998) and was the basic assumption behind the earliest conceptual and numerical models of ice shelf–ocean interaction (Doake 1976; Robin 1979; MacAyeal 1985; Jenkins and Doake 1991). Despite its simplicity, the application of such a boundary condition to an ocean model may not be straightforward. If the usual prognostic equations for temperature and salinity are solved everywhere, the derived values must subsequently be reset wherever the mixed layer is in contact with ice. The ''melt rate'' cannot be recovered from the boundary condition but is determined from the change in temperature of the mixed layer. The derived rate is therefore a function of model time step and mixed layer thickness among other things. This is an undesirable feature if the aim is an accurate diagnosis of the melting and, since this formulation is not directly comparable to those presented below, we will discuss it no further.

2) Two-equation formulations

The next approach that we will discuss recognizes that the rate at which the mixed layer temperature relaxes toward the freezing point is governed by the diffusion of heat through the oceanic boundary layer. Equation (2) is introduced and estimates are made of the two heat fluxes that appear on the left-hand side. In their most general form they can be written

$$Q_I^T = -\rho_I c_{pI} \kappa_I^T \frac{\partial T_I}{\partial z}\bigg|_B \tag{6}$$

and

$$Q_M^T = -\rho_M c_{pM} \kappa_M^T \frac{\partial T_M}{\partial z}\bigg|_B. \tag{7}$$

In the above equations κ are thermal diffusivities adjacent to the ice–ocean interface, ρ are densities, and c_p are specific heat capacities, while subscript M indicates mixed layer properties and I ice properties. In Eq. (6) the density, specific heat capacity, and thermal diffusivity may all be regarded as constant, and the problem becomes one of estimating the temperature gradient at the base of the ice shelf. To solve Eq. (7) we can treat the density and specific heat capacity as constant, but we need a suitable parameterization of the product of the diffusivity and temperature gradient near the ice shelf base. If the boundary layer were laminar, we would anticipate that the temperature would vary linearly between the interface and mixed layer temperatures, in which case Eq. (7) could be written

$$Q_M^T = -\rho_M c_{pM} \kappa_M^T \frac{(T_B - T_M)}{h}, \tag{8}$$

where h is the boundary layer thickness. Turbulence in

the boundary layer means that the temperature profile is nonlinear and the diffusivity is variable, but we can parameterize these complications with the introduction of a Nusselt number, Nu, an empirical parameter having a value greater than 1:

$$Q_M^T = -\rho_M c_{pM} \left(\frac{\mathrm{Nu}\kappa_M^T}{h}\right)(T_B - T_M). \tag{9}$$

We will refer to the first quantity in brackets, which has dimensions of velocity, as a thermal exchange velocity γ_T. The simplest approach would be to choose a constant value for the exchange velocity but, recognizing that it is a result of turbulence in the mixed layer, a more realistic assumption is to make it a function of the friction velocity.

The two-equation formulation offers some advantages over the one-equation formulation. It is still very simple, but it includes a diagnosis of the melt rate. Associated heat and freshwater fluxes can then be applied to the ocean model in an identical manner to all other surface fluxes, and no special treatment of the mixed layer equations is required because of the presence of ice. However, it still lacks some realism, as to solve Eq. (1) it must be assumed that the interface salinity and the mixed layer salinity are identical. This implies infinite salt diffusivity, whereas in reality we would expect salt to diffuse at the same rate as, or slower than, heat. Nevertheless, the only error implied by this assumption is the misdiagnosis of the interface temperature, and as this is a weak function of salinity, we might anticipate relatively small errors. McPhee (1992) and McPhee et al. (1999) show that this formulation produces heat fluxes that agree well with measurements made beneath sea ice having a wide range of roughness characteristics. An analogous formulation, but with a constant thermal exchange velocity and a constant, prescribed interface salinity, has been used in the sub-ice-shelf models of Determann and Gerdes (1994), Grosfeld et al. (1997), and Williams et al. (1998).

3) Three-equation formulations

The most sophisticated formulations make no prior assumptions about conditions at the interface and solve Eqs. (1), (2), and (5) using the known mixed layer and ice properties. By an analogous argument to that used in the derivation of Eq. (9) we can express the surviving term on the left-hand side of Eq. (5) as

$$Q_M^S = -\rho_M \gamma_S (S_B - S_M), \tag{10}$$

where γ_s is the salinity exchange velocity. Once again the exchange velocity can be either assumed constant or assigned a functional dependence on friction velocity. The former approach was followed by Hellmer and Olbers (1989, 1991), Scheduikat and Olbers (1990), and Hellmer and Jacobs (1992). The latter approach has been developed in the sea-ice literature [see Gade (1993) for

a review] and adopted in the ice shelf–ocean interaction models of Jenkins (1991), Jenkins and Bombosch (1995), Hellmer and Jacobs (1995), and Hellmer et al. (1999).

c. Parameterizing the transfer of heat and salt through the oceanic boundary layer

The key to diagnosing a realistic melt rate from either the two- or the three-equation formulation lies in the choice of appropriate exchange velocities. In the case of the three-equation model the problem is complicated by the fact that the thermal and salinity diffusivities can only be assumed to be equal in the fully turbulent part of the boundary layer. Close to the ice–ocean interface, the eddy size and hence the turbulent diffusivity are suppressed. Where the suppression is great enough that molecular diffusion becomes the dominant transfer mechanism, heat will diffuse more rapidly than salt. As the exchange velocities need to account for all processes occurring within the boundary layer, γ_s will be smaller than γ_T.

The role of molecular diffusion in governing the rate of heat and mass transfer within a thin, viscous sublayer adjacent to the ice–ocean boundary was recognized by Mellor et al. (1986). Subsequently, McPhee et al. (1987) and Steele et al. (1989) investigated boundary layer parameterizations that explicitly included a viscous sublayer. Jenkins (1991) used an analogous parameterization to calculate exchange velocities at the base of an ice shelf. Assuming the ice–ocean interface in this case to be hydraulically smooth leads to expressions of the form (Kader and Yaglom 1972)

$$\gamma_T = \frac{u_*}{2.12 \ln(u_* h/\nu) + 12.5 \ Pr^{2/3} - 9} \quad (11)$$

and

$$\gamma_S = \frac{u_*}{2.12 \ln(u_* h/\nu) + 12.5 \ Sc^{2/3} - 9}. \quad (12)$$

The influence of the molecular sublayer is apparent in the inclusion of the molecular Prandtl number, Pr (the ratio of viscosity to thermal diffusivity), and the molecular Schmidt number, Sc (the ratio of viscosity to salinity diffusivity), in the denominators. The kinematic viscosity of sea water is considered constant and is denoted by the symbol ν. The friction velocity u_* is defined in terms of the shear stress at the ice–ocean interface, a simple parameterization of which involves a dimensionless drag coefficient c_d and the velocity of the mixed layer U_M, the ice being considered stationary:

$$u_*^2 = c_d U_M^2. \quad (13)$$

A potentially important effect not accounted for in (11) and (12) is the impact of the buoyancy flux at the ice–ocean interface on turbulence within the boundary layer. A stabilizing buoyancy flux (i.e., melting) will suppress mixing, while a destabilizing buoyancy flux (i.e., freezing) will enhance mixing (McPhee 1994). We wish to investigate how the stability of the boundary layer might influence melt rates at the base of an ice shelf, so we follow McPhee et al. (1987) in expressing the transfer coefficients as

$$\gamma_{T,S} = \frac{u_*}{\Gamma_{Turb} + \Gamma_{Mole}^{T,S}}, \quad (14)$$

where

$$\Gamma_{Turb} = \frac{1}{k} \ln\left(\frac{u_* \xi_N \eta_*^2}{f h_\nu}\right) + \frac{1}{2 \xi_N \eta_*} - \frac{1}{k} \quad (15)$$

and

$$\Gamma_{Mole}^{T,S} = 12.5 (Pr, \ Sc)^{2/3} - 6. \quad (16)$$

In Eq. (15) k is von Kármán's constant, f is the Coriolis parameter, ξ_N is a dimensionless constant, and h_ν is the thickness of the viscous sublayer. Values for the first three of these are given in Table 1, while we estimate the sublayer thickness to be (Tennekes and Lumley 1972, p. 160)

$$h_\nu = 5 \frac{\nu}{u_*}. \quad (17)$$

In Eqs. (15)–(17) we have assumed the ice–ocean interface to be hydraulically smooth. The influence of the interfacial buoyancy flux is encapsulated in the stability parameter, introduced by McPhee (1981):

$$\eta_* = \left(1 + \frac{\xi_N u_*}{f L_O R_c}\right)^{-1/2}, \quad (18)$$

where R_c is a critical flux Richardson number and L_o is the Obukhov length. If the Obukhov length is negative (i.e., the buoyancy flux is destabilizing) the stability parameter is set to 1. We do not consider how destabilizing buoyancy fluxes influence freezing rates because direct freezing to the ice shelf base is thought to be limited. The formation of frazil ice in the water column, which we do not discuss here, will have a stabilizing effect on the boundary layer (Jenkins and Bombosch 1995).

d. Modeling the heat flux into the ice shelf

We now address the problem of estimating the basal temperature gradient in the ice shelf, required in Eq. (6). This requires solution of the heat transport equation in the ice shelf:

$$\frac{\partial T_I}{\partial t} + \mathbf{U}_I \cdot \nabla T_I = \kappa_I^T \nabla^2 T_I. \quad (19)$$

In practice, the solution of the full equation is not possible unless the flow field within the ice shelf is known, so we consider reduced forms.

1) NO ADVECTION, NO DIFFUSION

The simplest of all approximations is that the ice shelf is a perfect insulator. With no diffusion into the ice shelf, the first term on the left-hand side of Eq. (2) is identically zero. Such an approximation has been used by Determann and Gerdes (1994), Jenkins and Bombosch (1995), Grosfeld et al. (1997), and Williams et al. (1998), although it can be justified only if the conducted heat flux is always small compared to the latent heat term.

2) NO ADVECTION, VERTICAL DIFFUSION

In this case (19) reduces to

$$\frac{\partial^2 T_I}{\partial z^2} = 0 \qquad (20)$$

for a steady state. The solution is a linear temperature profile throughout the thickness of the ice shelf, so the basal gradient can be expressed as

$$\left.\frac{\partial T_I}{\partial z}\right|_B = \frac{(T_S - T_B)}{H_I}, \qquad (21)$$

where H_I is the thickness of the ice shelf and T_S is the surface temperature. Such an approximation has been used in the models of Hellmer and Olbers (1989, 1991), Scheduikat and Olbers (1990), and Hellmer and Jacobs (1992, 1995). This approach is common in sea–ice models, but the thickness of ice shelves and the observed, highly nonlinear temperature profiles make it less satisfactory for modeling ice-shelf thermodynamics.

3) CONSTANT VERTICAL ADVECTION, VERTICAL DIFFUSION

The simplest way to allow a nonlinear temperature profile to develop is to allow for vertical advection within the ice shelf. We will assume that the vertical velocity is constant and equal to the basal melt/freeze rate and that the ice shelf is in a steady state. There is some justification for this approximation in that over the short timescales of interest here, that is, of years to decades, the ice shelves are believed to be in a relatively steady state. Clearly, such an approximation would be unrealistic for consideration of sea ice thermodynamics because of its thinness. This requires that all ice added or removed at the base is balanced by surface ablation or accumulation. In this case Eq. (19) reduces to the equation used by Wexler (1960) (see also discussion by Paterson 1994, p. 204):

$$\frac{\partial^2 T_I}{\partial z^2} + \frac{w_I}{\kappa_I^T}\frac{\partial T_I}{\partial z} = 0, \qquad (22)$$

where
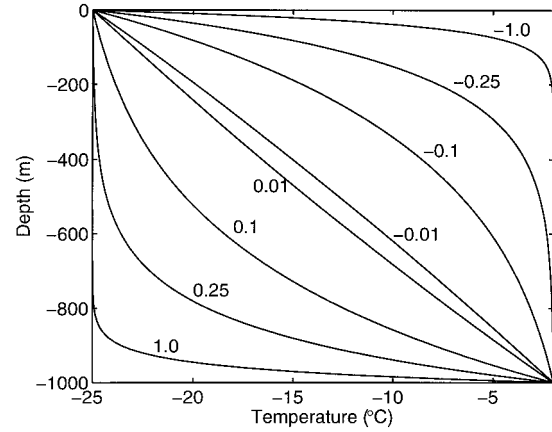
$$w_I = \frac{\rho_M}{\rho_I}w_B. \qquad (23)$$

FIG. 2. Temperature–depth profiles through an ice shelf 1000 m thick, calculated assuming a constant vertical velocity. Surface and basal temperatures are $-25°$ and $-2°$C, respectively. Vertical velocity (in m yr^{-1}) is given for each profile where positive labels indicate basal melting.

We assume a solution of the form $T(z) = e^{mz}$, which yields a quadratic characteristic polynomial of Eq. (22) having the two roots $m_1 = -w_I/\kappa_I^T$ and $m_2 = 0$. The general solution of Eq. (22) is then

$$T_I(z) = c_1 e^{m_1 z} + c_2 e^{m_2 z}, \qquad (24)$$

where c_1 and c_2 are constants to be determined by the boundary conditions of fixed temperatures at the ice shelf surface T_S and base T_B. Utilizing these boundary conditions, the temperature profile can be written

$$T_I(z) = \frac{(T_S - T_B)\exp\left(\dfrac{-w_I z}{\kappa_I^T}\right) + T_B - T_S\exp\left(\dfrac{w_I H_I}{\kappa_I^T}\right)}{1 - \exp\left(\dfrac{w_I H_I}{\kappa_I^T}\right)} \qquad (25)$$

with $z = 0$ at the surface and $z = -H_I$ at the base. The solution expressed by (25) is shown in Fig. 2 for an ice shelf 1000 m thick experiencing a range of basal melting and freezing rates. Under melting conditions, the temperature gradient near the base of the ice shelf is increased, which increases the conductive heat flux and serves to counteract the melting. Conversely, freezing decreases the temperature gradient and the conductive flux, which leads to a lower freezing rate than would be estimated for a linear temperature profile.

From Eq. (25) we can derive the temperature gradient at the ice shelf base:

$$\left.\frac{\partial T_I}{\partial z}\right|_B = \Pi\frac{(T_S - T_B)}{H_I}. \qquad (26)$$

Equation (26) has the same form as Eq. (21) apart from the factor

$$\Pi = \frac{\Upsilon}{e^{\Upsilon} - 1}, \qquad (27)$$

which depends on the Péclet number

$$\Upsilon = \frac{-w_I H_I}{\kappa_I^T}. \qquad (28)$$

For a melt rate of 1 m yr^{-1} at the base of an ice shelf 1000 m thick we obtain a Péclet number of approximately -30, implying that the temperature gradient amplification factor Π can play an important role in Eq. (26).

Immediately obvious is that Eq. (27) is ill-defined for a melt rate of zero, a problem that may be overcome by rewriting the right-hand side as a power series (Arfken 1970) of the form

$$\frac{\Upsilon}{e^{\Upsilon} - 1} = \sum_{n=0}^{\infty} B_n \frac{\Upsilon^n}{n!}, \qquad (29)$$

where B_n represent the sequence of Bernoulli numbers. The first few Bernoulli numbers have values (Abramowitz and Stegun 1972)

$$B_0 = 1, \qquad B_2 = -\frac{1}{2}, \qquad B_4 = -\frac{1}{30},$$

$$B_6 = \frac{1}{42}, \cdots \qquad (30)$$

the odd labeled Bernoulli numbers, B_{2n+1} for $n = 1, 2, 3, \ldots$, being identically zero. The series (29) is valid for $\Upsilon < 2\pi$ and is therefore appropriate for small values of the Péclet number (i.e., a near-zero melt/freeze rate). In particular when $\Upsilon = 0$, the expression in (29) equals B_0 and Eq. (26) is then identical to Eq. (21), the purely diffusive solution with no advection. We also note that for sea ice $\Upsilon < 1$ typically, so the purely diffusive solution is a good approximation.

Figure 3 illustrates the behavior of Π as a function of the Péclet number. Under conditions of moderate to high freezing Π is close to zero, while for moderate to high melting it is very close to the absolute value of the Péclet number. This suggests that a possible simplification of Eq. (27) is

$$\Pi = \begin{cases} \dfrac{w_I H_I}{\kappa_I^T} & \text{for melting case when } w_B > 0 \\[2mm] 0 & \text{for freezing case when } w_B < 0. \end{cases} \qquad (31)$$

This approximation (also shown in Fig. 3) has the advantage of linearizing Eq. (2), and hence simplifying the solution of the ice–ocean boundary equations. Such an approximation was introduced by Nøst and Foldvik (1994) and has been adopted in the model of Hellmer et al. (1999).

4) MORE COMPLEX MODELS

The next stage of complexity in the heat transport problem would be to introduce a vertical velocity that
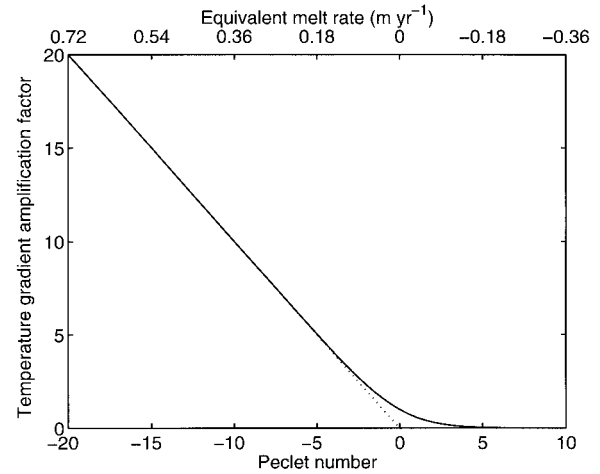

FIG. 3. Temperature gradient amplification factor as a function of Péclet number. The dotted line shows the approximation given in Eq. (31). The upper axis scale indicates equivalent melt rates for an ice shelf 1000 m thick.

varies linearly from the surface to the base of the ice shelf. This would lead to the classical solution for the temperature profile in an ice column, first introduced by Robin (1955) for ice sheets. However, the solution involves either error functions or Dawson's integrals, and we have little hope of recovering a linear version of Eq. (2). To use such a solution, the basal temperature gradient would have to be calculated as a separate problem and the result introduced directly into Eq. (6). The same applies to models of greater sophistication that could include the horizontal advection of heat. Such a model was used by Jenkins (1991) for a specific region of Ronne Ice Shelf where measurements of ice flow and surface temperature made the computation of a steady-state temperature distribution within the ice shelf possible.

3. Comparison of model results

We begin by discussing the behavior of the three-equation formulations, which are the most widely used in the literature on ice shelf–ocean interactions, and we will initially treat the ice shelf as a perfect insulator. With no heat conduction into the ice shelf, the only external parameters that enter into Eqs. (1), (2), and (5) are the friction velocity u_* and the thermal driving T_*, defined as

$$T_* = T_M - (aS_M + b + cp_B). \qquad (32)$$

The difference between the various formulations lies in the specification of the exchange velocities for heat and salt, which are illustrated in Fig. 4. The two formulations that include an explicit parameterization of the boundary layer yield heat transfer coefficients that are approximately linear functions of friction velocity, with values that generally differ by no more than about 10% (Fig.
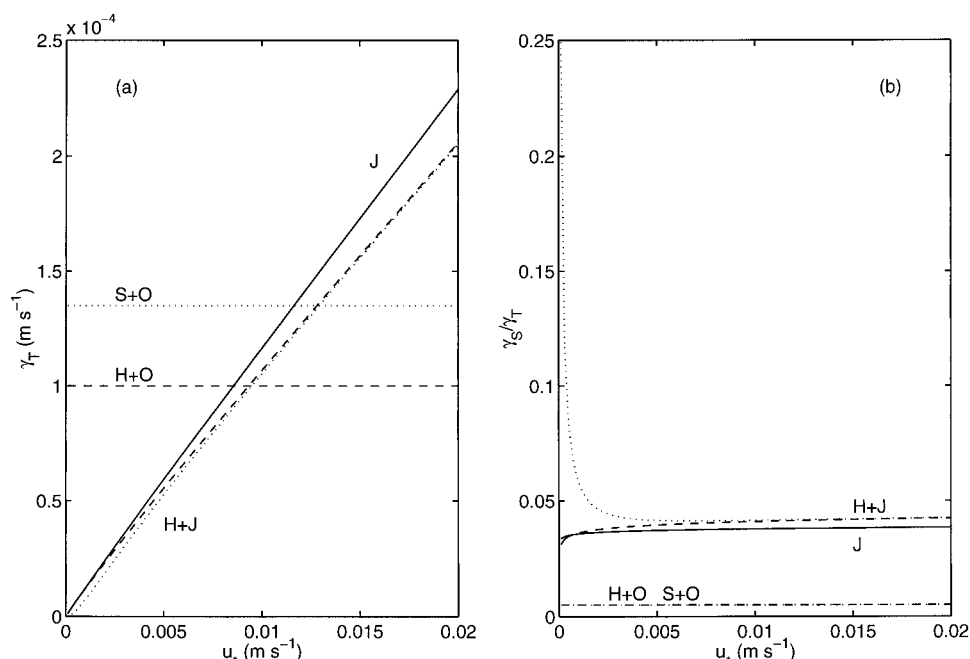
FIG. 4. (a) Heat transfer coefficients introduced by Hellmer and Olbers (1989) (dashed line labeled H+O), by Scheduikat and Olbers (1990) (dotted line labeled S+O), by Jenkins (1991) (solid line labeled J), and in this paper (dotted and dashed lines labeled H+J). In the latter case the dashed line indicates values obtained with the stability parameter of Eq. (18) set to 1, while the dotted line indicates values for a melt rate of 10 m yr^{-1}. (b) Ratio of salt to heat transfer coefficients for the same formulations.

4a). The reason for this close agreement is the dominance of the molecular term, which is the same in all cases, in the denominators of Eqs. (11) and (14). The two models having constant exchange velocities use values of γ_T that are consistent with a friction velocity of about 0.01 m s^{-1}, which corresponds to a mixed layer velocity of about 0.2 m s^{-1}. Although this is higher than most estimates of currents associated with the thermohaline circulation, it is consistent with rms currents associated with strong tidal flow (Makinson and Nicholls 1999). That the ratio of γ_s to γ_T is significantly less than one in all cases, and is relatively constant in most, (Fig. 4b) is evidence of the importance of molecular processes. Heat and salt transfer within the turbulent part of the boundary layer has little impact on the size of the coefficients except in the formulation that considers the influence of gravitational stability, and even in this formulation the effect is only significant under conditions of high thermal driving and low friction velocity.

A model's response to thermal driving is determined by the magnitudes of both the heat and the salt transfer coefficients. Figures 5a–c show the influence of changing the size of both γ_S and γ_T while keeping their ratio constant. Temperature and salinity differences across the boundary layer are set entirely by the thermal driving, with computed melt rates then responding linearly to variations in γ_S and γ_T, as heat and salt are transported with varying ease across the boundary layer. This re-

sponse is similar to what we would anticipate for a two-equation formulation. However, the salinity difference across the boundary layer (Fig. 5c) means that the corresponding temperature difference (Fig. 5b) is always smaller than the thermal driving. Calculated melt/freeze rates are therefore lower than they would be if the boundary salinity were assumed to be equal to the mixed layer salinity. There is also a slight nonlinearity in the response to thermal driving that arises because the salinity at the ice–ocean interface can increase without limit but can only decrease by ~35 psu before becoming completely fresh.

The role played by salinity diffusion in determining the melt/freeze rates is shown more clearly in Figs. 5d–f, where the effect of varying the ratio of γ_S to γ_T while keeping the latter constant is illustrated. As the ratio tends to infinity, the response becomes that of a two-equation formulation with zero salinity difference across the boundary layer (Fig. 5f), a temperature difference equal to the thermal driving (Fig. 5e), and a melt/freeze rate that is directly proportional to T_* (Fig. 5d). Decreasing the salinity diffusivity increases the salinity difference across the boundary layer, which decreases the temperature difference and with it the melt/freeze rate, while the nonlinearity in the response to T_* becomes more pronounced. With negative thermal driving, the salinity at the boundary can grow until the freezing point depression balances the thermal driving, yielding a temperature difference of zero across the boundary
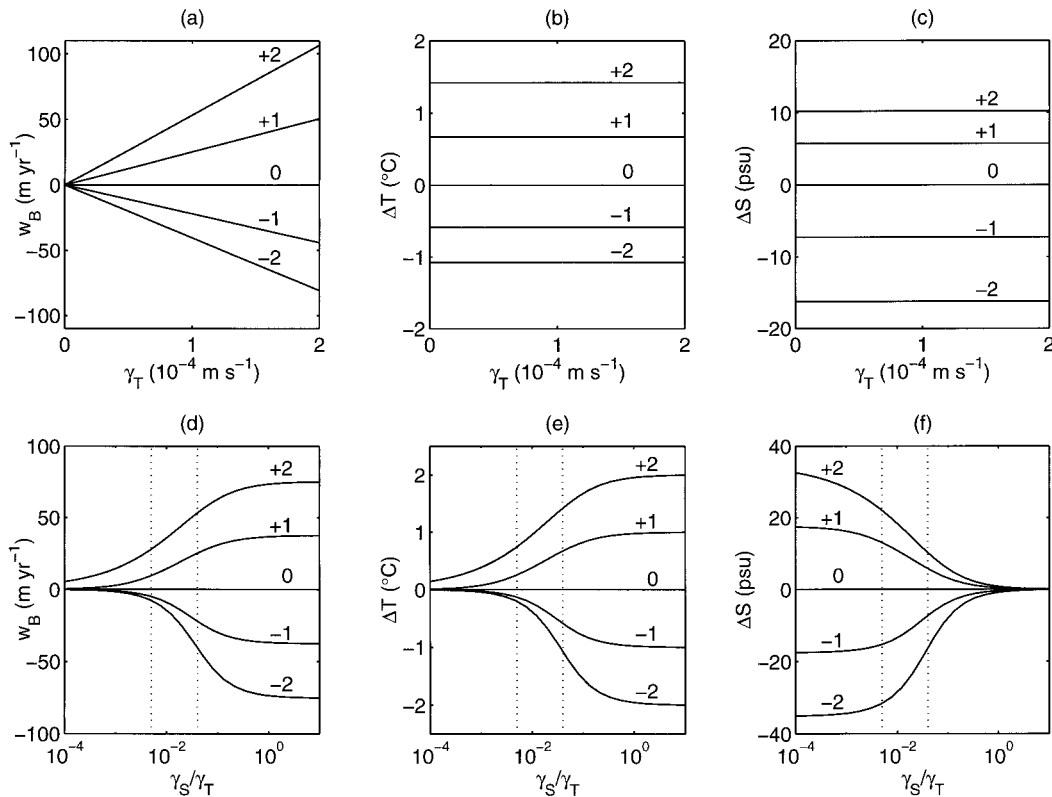
FIG. 5. Response of a three-equation formulation for thermal driving of $+2°$, $+1°$, $0°$, $-1°$, and $-2°C$ plotted against the magnitude of the thermal exchange velocity γ_T, (a) melt rate, (b) temperature difference across the boundary layer, (c) salinity difference across the boundary layer. The ratio of the salinity exchange velocity γ_s to γ_T is kept at 0.04. Panels (d), (e), and (f) show the response of the same variables to changes in the ratio of γ_s to γ_T, while the latter is kept constant at 1.0×10^{-4} m s^{-1}. The dotted lines indicate ratios typical of formulations with constant coefficients (0.005) and those based on boundary layer parameterizations (0.04).

layer and hence no freezing, but, given sufficient positive thermal driving, melting can proceed even if the water at the boundary is completely fresh. The two values of γ_s/γ_T found in the literature span a region of high sensitivity. The lower ratio gives rise to melting and freezing rates that are not only smaller (for the same heat transfer coefficient), but also show a more nonlinear response to thermal driving.

The effects discussed above are illustrated quantitatively in Fig. 6, which shows the melt/freeze rates computed by each of the models for a broad range of thermal driving. The two boundary layer parameterizations give rather similar results, suggesting that the precise form of Γ_{Turb} is not critical. This is convenient, as the introduction of the stability parameter into Eq. (15) involves a computationally expensive iteration to derive the melt rates and exchange coefficients. Simply setting the stability parameter to unity does not have a large impact on melt rates computed with this model, except at very low friction velocity (Fig. 7a). For thermal driving less than 0.5°C (i.e., values commonly found in nature) and a friction velocity greater that 0.001 (corresponding to a velocity of about 0.02 m s^{-1}) differences between melt

rates computed with and without the stability parameter differ by less than 10%.

A possible refinement to the models discussed above would be the introduction of a conductive heat flux into the ice shelf. The influences of purely diffusive and constant vertical advection/diffusion models are illustrated in Figs. 7b,c. The linear temperature profile assumed by the purely diffusive model causes a net shift toward freezing so that a positive thermal driving is required for zero melting. Only in the region of the melt/freeze transition, where the rates are very small, does this approximation have a noticeable impact on model results (Fig. 7b). The model with constant vertical heat advection in the ice shelf has no effect unless the mixed layer is warmer than the freezing point. It then reduces the computed melt rates by about 10% (Fig. 7c).

McPhee (1992) and McPhee et al. (1999) demonstrated that direct measurements of the turbulent heat flux in the boundary layer beneath drifting sea ice could be well fitted with a two-equation model. This might be anticipated from the approximately linear response of the three-equation models, particularly at the moderate levels of thermal driving that are of most practical
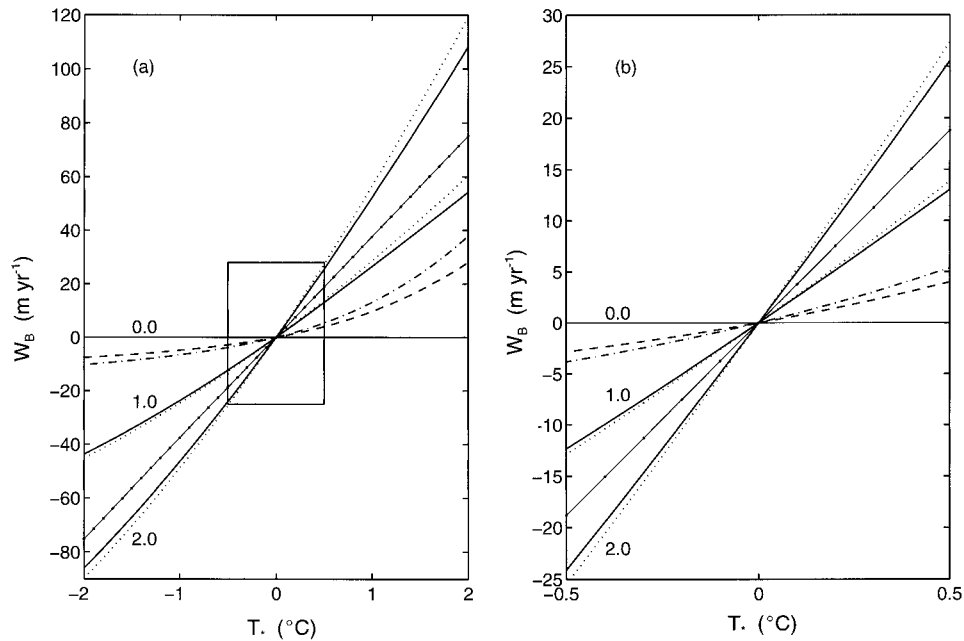
FIG. 6. Melt/freeze rates as a function of thermal driving calculated using exchange velocities given by Eqs. (14)–(18) (solid lines), by Jenkins (1991) (dotted lines), by Hellmer and Olbers (1989) (dashed line), by Scheduikat and Olbers (1990) (dot–dashed line), and by Determann and Gerdes (1994) (solid line with dots). In the Jenkins and Hellmer and Olbers cases, three curves are shown and labeled for friction velocities of 0.0, 1.0, and 2.0 cm s^{-1}. Panel (b) shows an enlargement of the boxed area in panel (a).

interest (Fig. 6b). However, the key to a consistent two-equation formulation lies in the choice of an effective exchange velocity, which accounts approximately for the fact that the finite salinity diffusivity supports a salinity difference across the boundary layer and hence reduces the thermal forcing. Using Eq. (1) we can rewrite Eq. (32) as

$$T_* = (T_M - T_B) - a (S_M - S_B) \quad (33)$$

from which we can express the ratio of thermal driving (T_*) to thermal forcing $(T_M - T_B)$ as

$$\Theta = 1 - a \frac{(S_M - S_B)}{(T_M - T_B)}. \quad (34)$$

From Eqs. (2) and (5), with all fluxes into the ice shelf ignored, Eq. (34) can be written

$$\Theta = 1 - \frac{aS_B c_{pM} \gamma_T}{L_f \gamma_S}. \quad (35)$$

Provided this factor is approximately constant, a two-equation formulation with an effective transfer coefficient of γ_T/Θ should yield reasonable melt rates. Taking $S_B = 34.5$ psu gives $\Theta = 1.6$ for $\gamma_S/\gamma_T = 0.04$, typical for the models of Jenkins (1991) and McPhee et al. (1987), and $\Theta = 5.7$ for $\gamma_S/\gamma_T = 0.005$, as in the models of Hellmer and Olbers (1989) and Scheduikat and Olbers (1990).

Figure 7d illustrates the differences between melting/freezing rates calculated with the model that includes the stability parameter and those derived from an equivalent two-equation formulation. We find large differences for high thermal driving, particularly at low values of the friction velocity, most of which are a result of ignoring the effect of stability (Fig. 7a). At higher friction velocity, the linear response of the two-equation formulation means that melting rates tend to be underestimated and freezing rates overestimated compared with the results of the full three-equation model. However, for conditions frequently encountered in nature $(|T_*| < 0.5°C, u_* > 0.001)$ differences between the two- and three-equation formulations are typically less than 10%.

In Fig. 8 we compare the effective transfer coefficients for each of the formulations discussed above, with that derived by McPhee et al. (1999) from observations in the turbulent boundary layer beneath sea ice. The models of McPhee et al. (1987) and Jenkins (1991) reproduce the observed dependency on friction velocity, but overestimate turbulent transfer by about 15% and 30%, respectively. The constant transfer coefficients used by Hellmer and Olbers (1989) and Scheduikat and Olbers (1990) are consistent with currents of 0.06–0.08 m s^{-1}, the right order of magnitude for the thermohaline-forced circulation beneath ice shelves. The effective transfer coefficient of Determann and Gerdes (1994) is much higher, corresponding to a velocity of about 0.35 m s^{-1}, and is therefore appropriate for a cavity subject to vigorous tidal mixing. The melt/freeze rates produced by this latter model are shown in Fig. 6 for comparison.
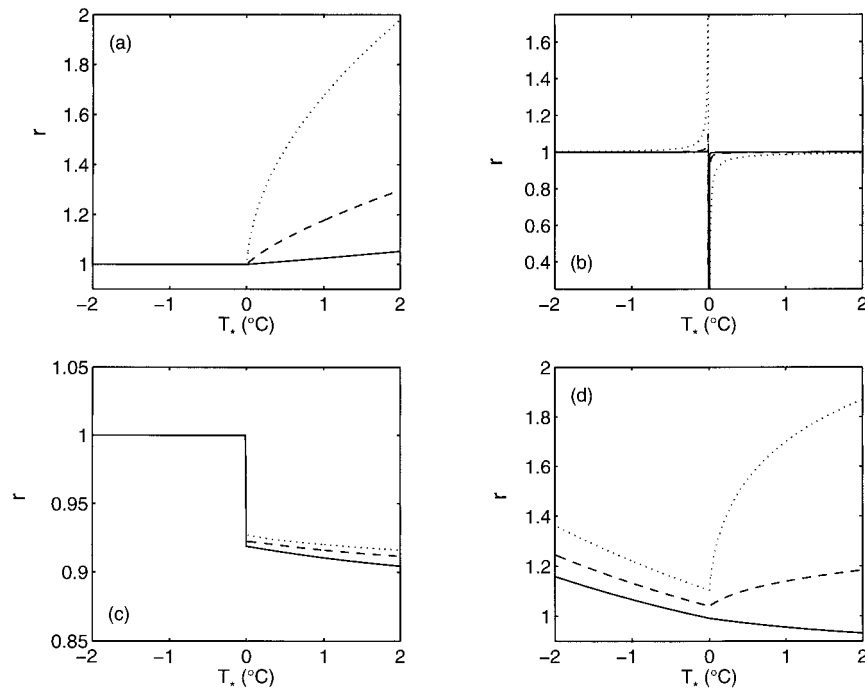
FIG. 7. Ratio of the melt/freeze rate r derived from different formulations to that calculated using the standard three-equation formulation with exchange velocities set according to Eqs. (14)–(18) and no heat conduction into the ice shelf. In each panel, solid lines indicate results obtained with a friction velocity of 1 cm s^{-1}, dashed lines with 0.1 cm s^{-1}, and dotted lines with 0.01 cm s^{-1}. The different formulations are (a) exchange velocities derived from Eqs. (14)–(18) with the stability parameter set to 1, (b) the standard model with vertical heat diffusion in the ice shelf, (c) the standard model with vertical advection and diffusion of heat in the ice shelf, and (d) an equivalent two-equation formulation. Note that the vertical scale differs between panels.
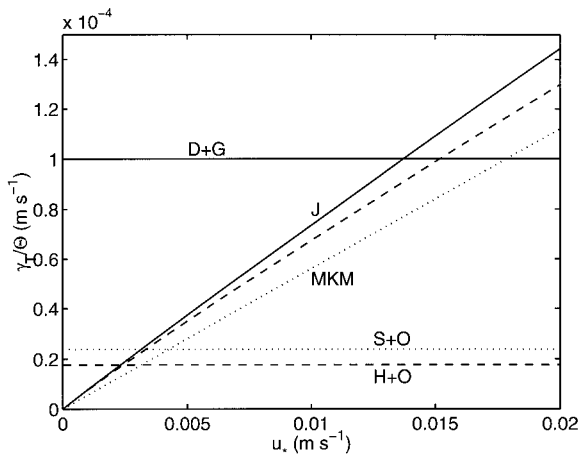

FIG. 8. Effective transfer coefficients for the formulations introduced by Hellmer and Olbers (1989) (dashed line labeled H+O), by Scheduikat and Olbers (1990) (dotted line labeled S+O), by Jenkins (1991) (solid line labeled J), in this paper (unlabeled, dashed line), and by Determann and Gerdes (1994) (solid line labeled D+G). The dotted line labeled MKM illustrates the effective transfer coefficient derived by McPhee et al. (1999) based on observations.

4. Computed buoyancy fluxes

Buoyancy fluxes associated with melting and freezing represent the primary forcing on the ocean beneath an ice shelf. Here we analyze how the differing formulations of the ice–ocean interaction discussed above influence the forcing imparted to an ocean model. The rate of change of mixed layer buoyancy can be written

$$\dot{B}_M = -g\beta_S \dot{S}_M \left(1 - \frac{\beta_T \dot{T}_M}{\beta_S \dot{S}_M} \right), \qquad (36)$$

where β_S and β_T are the salinity contraction and thermal expansion coefficients, respectively. The term outside the brackets is directly related to the freshwater flux associated with melting:

$$\dot{S}_M = -\frac{S_M}{H_M} w_B, \qquad (37)$$

where H_M denotes the thickness of the mixed layer. The term in brackets can be rewritten

$$\frac{\beta_T \dot{T}_M}{\beta_S \dot{S}_M} = \frac{(\partial T/\partial S)_M}{(\partial T/\partial S)_\sigma}. \qquad (38)$$

Melting of ice into the mixed layer causes its T/S properties to evolve along a straight line, the gradient of

which has been derived by Gade (1979), Greisman (1979), and Nøst and Foldvik (1994), and appears as the numerator on the right-hand side of Eq. (38). The denominator is the isopycnal slope in T/S space. Of relevance to the discussion here is that $(\partial T/\partial S)_M$ depends on the assumptions made about the heat flux into the ice shelf (Nøst and Foldvik 1994). In particular, the advection/diffusion model yields a $(\partial T/\partial S)_M$ of 2.8 (for a surface temperature of $-25°C$), while the commonly used model of a perfectly insulating ice shelf gives a value that is lower by 0.33. The overall error in buoyancy forcing is

$$\delta \dot{B}_M = \delta w_B \frac{\partial \dot{B}_M}{\partial w_B} + \delta(\partial T/\partial S)_M \frac{\partial \dot{B}_M}{\partial(\partial T/\partial S)_M} \quad (39)$$

from which we obtain

$$\frac{\delta \dot{B}_M}{\dot{B}_M} = \frac{\delta w_B}{w_B} + \frac{\delta(\partial T/\partial S)_M}{(\partial T/\partial S)_\sigma - (\partial T/\partial S)_M}. \quad (40)$$

As expected, we find that any model that gives an error in the melt rate contributes the same percentage error to the buoyancy forcing. However, if the melt rate is misdiagnosed because of an error in the estimate of the heat conducted into the ice shelf, there is an additional error in the forcing. Figure 7c shows a 10% difference between the melt rates derived from a model having constant vertical advection in the ice shelf and those derived with a model that treats the ice as a perfect insulator. The additional error in buoyancy forcing, arising from the second term on the right-hand side of Eq. (40), is small ($\sim$1%) near the surface, where the isopycnals are steep, but rises to about 5% at a depth of 2000 m, which is reached beneath the thickest ice shelves.

5. Summary and conclusions

The main objective of this study has been the presentation of an hierarchy of models describing the thermodynamic interaction between the base of an ice shelf and the underlying ocean waters. We have reviewed the various models that have been used in the literature on ice shelf–ocean interactions and have introduced a parameterization of turbulent transfer in the oceanic boundary layer, based on the work of McPhee et al. (1987), that considers the impact of gravitational stability. We have investigated the behavior of all the models and analyzed their performance in the light of recent studies of the turbulent boundary layer beneath sea ice (McPhee 1992; McPhee et al. 1999). A key finding of the latter authors is that turbulent transfer is apparently independent of the roughness of the ice–ocean interface, a fact that gives us confidence in extrapolating their findings to an ice shelf base of unknown roughness.

Most of the models in the literature conform to the three-equation formulation, although the choice of thermal and salinity transfer coefficients varies. We have

shown that the behavior of these models can be approximated by an equivalent two-equation formulation, at least for moderate thermal driving. The nonlinearity in the response of the three-equation models, a feature that does not appear in the simpler formulation, only becomes apparent at high thermal driving. In nature, supercooling can always be damped by the formation of frazil ice within the water column (Jenkins and Bombosch 1995), making model behavior at negative thermal driving greater than $\sim$0.1°C of theoretical rather than practical interest. Conditions of high positive thermal driving are unlikely to be encountered beneath the ice shelves of the Ross and Weddell Seas, but measurements from beneath George VI Ice Shelf, in the Bellingshausen Sea, show water more than 1°C above freezing within a few meters of the ice shelf base (K. W. Nicholls 1998, personal communication). A two-equation formulation may be inappropriate under these conditions, which may require the use of the full model of McPhee et al. (1987).

We have discussed various parameterizations of the heat flux into the ice shelf. The only one that manages to capture any of the nonlinearity of the typical ice shelf temperature profile is that which assumes constant vertical advection of ice. Applying this parameterization reduces melting by about 10% but reduces the buoyancy forcing on the ocean by up to 15%, the additional change being the result of the heat loss to the overlying ice. The overall effect is comparable to the differences in buoyancy forcing associated with the various choices of transfer coefficients used in the three-equation models. In nature, the temperature distribution within an ice shelf is determined by the history of melting and freezing that each ice column has experienced, but to introduce this thermal memory of past conditions would require a rather sophisticated dynamic/thermodynamic model of the ice shelf.

Our most important results are summarized in Figs. 6 and 8, which illustrate the behavior of the models used to date in the literature on ice shelf–ocean interactions. The three-equation models of Hellmer and Olbers (1989) and Scheduikat and Olbers (1990) have effective transfer coefficients that are only one-fifth the size of that used by Determann and Gerdes (1994). In the models of Jenkins (1991) and Jenkins and Bombosch (1995), typical friction velocities lie in the range 0.002–0.008 m s^{-1}, yielding effective transfer coefficients ranging in magnitude from that of Hellmer and Olbers (1989) up to half that used by Determann and Gerdes (1994). Whether it is better to use constant coefficients, ones based on assumed tidal velocities, or ones based on computed thermohaline velocities is an open question. However, when comparing model output, it is important to realize that the differing parameterizations of the ice–ocean interaction yield melting rates and hence buoyancy fluxes, that vary over a factor of 5 for the same thermal driving. Our recommendation is that formulations used in future, whether two-equation or three-

equation, should aim to reproduce the behavior observed by McPhee (1992) and McPhee et al. (1999), at least until such time as measurements of turbulent heat flux beneath ice shelves are available.

REFERENCES

Abramowitz, M., and I. A. Stegun, 1972: *Handbook of Mathematical Functions.* Dover p. 810.

Arfken, G., 1970: *Mathematical Methods for Physicists.* Academic Press, p. 279.

Bombosch, A., and A. Jenkins, 1995: Modeling the formation and deposition of frazil ice beneath the Filchner-Ronne Ice Shelf. *J. Geophys. Res.,* **100,** 6983–6992.

Determann, J. M., and R. Gerdes, 1994: Melting and freezing beneath ice shelves: Implications from a three-dimensional ocean-circulation model. *Ann. Glaciol.,* **20,** 413–419.

Doake, C. S. M., 1976: Thermodynamics of the interaction between ice shelves and the sea. *Polar Rec.,* **18,** 37–41.

Eicken, H., H. Oerter, H. Miller, W. Graf, and J. Kipfstuhl, 1994: Textural characteristics and impurity content of meteoric and marine ice in the Ronne Ice Shelf, Antarctica. *J. Glaciol.,* **40,** 386–398.

Fahrbach, E., R. G. Peterson, G. Rohardt, P. Schlosser, and R. Bayer, 1994: Suppression of bottom water formation in the southeastern Weddell Sea. *Deep-Sea Res.,* **41,** 389–411.

Foldvik, A., T. Gammelsrod, and T. Torresen, 1985: Circulation and water masses on the southern Weddell Sea shelf. *Oceanology of the Antarctic Continental Shelf,* S. S. Jacobs, Ed., *Antarct. Res. Ser.,* Vol. 43, Amer. Geophys. Union, 5–20.

Gade, H. G., 1979: Melting of ice in sea water: A primitive model with applications to the Antarctic ice shelf and icebergs. *J. Phys. Oceanogr.,* **9,** 189–198.

——, 1993: When ice melts in sea water: A review. *Atmos.–Ocean.,* **31,** 139–165.

Gill, A. E., 1973: Circulation and bottom water production in the Weddell Sea. *Deep-Sea Res.,* **20,** 111–140.

Greisman, P., 1979: On meltwater driven by the melt of ice shelves and tidewater glaciers. *Deep-Sea Res.,* **26,** 1051–1065.

Grosfeld, K., R. Gerdes, and J. Determann, 1997: Thermohaline circulation and interaction between ice shelf cavities and the adjacent open ocean. *J. Geophys. Res.,* **102,** 15 595–15 610.

Hellmer, H. H., and D. J. Olbers, 1989: A two-dimensional model for the thermohaline circulation under an ice shelf. *Antarc. Sci.,* **1,** 325–336.

——, and ——, 1991: On the thermohaline circulation beneath the Filchner-Ronne Ice Shelves. *Antarc. Sci.,* **3,** 433–442.

——, and S. S. Jacobs, 1992: Ocean interaction with the base of Amery Ice Shelf, Antarctica. *J. Geophys. Res.,* **97,** 20 305–20 317.

——, and ——, 1995: Seasonal circulation under the eastern Ross Ice Shelf, Antarctica. *J. Geophys. Res.,* **100,** 10 873–10 885.

——, ——, and A. Jenkins, 1999: Oceanic erosion of a floating Antarctic glacier in the Amundsen Sea. *Deep-Sea Res.,* in press.

Holland, D. M., 1998: On the parameterization of basal heat flux for sea-ice modelling. *Geophysica,* **34,** 1–21.

Holland, M. M., J. A. Curry, and J. L. Schramm, 1997: Modeling the thermodynamics of a sea ice thickness distributions 2: Sea ice/ocean interactions. *J. Geophys. Res.,* **102,** 23 093–23 107.

Jacobs, S. S., R. G. Fairbanks, and Y. Horibe, 1985: Origin and evolution of water masses near the Antarctic continental margin: Evidence from H₂¹⁸O/H₂¹⁶O ratios in sea water. *Oceanology of the Antarctic Continental Shelf,* S. S. Jacobs, Ed., *Antarctic Res. Ser.,* Vol. 43, Amer. Geophys. Union, 59–85.

Jenkins, A., 1991: A one dimensional model of ice-shelf ocean interaction. *J. Geophys. Res.,* **96,** 20 671–20 677.

——, and C. S. M. Doake, 1991: Ice ocean interaction on Ronne Ice Shelf, Antarctica. *J. Geophys. Res.,* **96,** 791–813.

——, and A. Bombosch, 1995: Modeling the effects of frazil ice crystals on the dynamics and thermodynamics of ice shelf water plumes. *J. Geophys. Res.,* **100,** 6967–6981.

Kader, B. A., and A. M. Yaglom, 1972: Heat and mass transfer laws for fully turbulent wall flows. *Int. J. Heat Mass Transfer,* **15,** 2329–2351.

MacAyeal, D. R., 1985: Evolution of tidally triggered melt water plumes below ice shelves. *Oceanology of the Antarctic Continental Shelf,* S. S. Jacobs, Ed., *Antarctic Res. Ser.,* Vol. 43, Amer. Geophys. Union, 133–143.

Makinson, K., and K. W. Nicholls, 1999: Modeling tidal currents beneath Filchner–Ronne Ice Shelf and on the adjacent continental shelf: Their effects on mixing and transport. *J. Geophys. Res.,* in press.

McPhee, M. G., 1981: An analytical similarity theory for the planetary boundary layer stabilized surface buoyancy. *Bound.-Layer Meteor.,* **21,** 325–339.

——, 1992: Turbulent heat fluxes in the upper ocean under sea ice. *J. Geophys. Res.,* **97,** 5365–5379.

——, 1994: On the turbulent mixing length in the oceanic boundary layer. *J. Phys. Oceanogr.,* **24,** 2014–2031.

——, G. A. Maykut, and J. H. Morison, 1987: Dynamics and thermodynamics of the ice/upper ocean system in the marginal ice zone of the Greenland Sea. *J. Geophys. Res.,* **92,** 7017–7031.

——, C. Kottmeier, and J. H. Morison, 1999: Ocean heat flux in the central Weddell Sea during winter. *J. Phys. Oceanogr.,* **29,** 1166–1179.

Mellor, G. L., M. G. McPhee, and M. Steele, 1986: Ice–seawater turbulent boundary layer interaction with melting and freezing. *J. Phys. Oceanogr.,* **6,** 1829–1846.

Millero, F. J., 1978: Annex 6: Freezing point of seawater. Eighth report of the joint panel of oceanographic tables and standards. *UNESCO Tech. Paper Mar. Sci.,* **28,** 29–31.

Nøst, O. A., and A. Foldvik, 1994: A model of ice shelf ocean interaction with application to the Filchner-Ronne and Ross Ice shelves. *J. Geophys. Res.,* **99,** 14 243–14 254.

Oerter, H., J. Kipfstuhl, J. Determann, H. Miller, D. Wagenbach, A. Minikin, and W. Graf, 1992: Evidence for basal marine ice in the Filchner-Ronne ice shelf. *Nature,* **358,** 399–401.

Omstedt, A., and U. Svensson, 1984: Modeling supercooling and ice formation in an Ekman layer. *J. Geophys. Res.,* **89,** 735–744.

Paterson, W. S. B., 1994: *The Physics of Glaciers.* Pergamon, 480 pp.

Robin, G. de Q., 1955: Ice movement and temperature distribution in glaciers and ice sheets. *J. Glaciol.,* **2,** 523–532.

——, 1979: Formation, flow and disintegration of ice shelves. *J. Glaciol.,* **24,** 259–271.

Scheduikat, M., and D. J. Olbers, 1990: A one-dimensional mixed layer model beneath the Ross Ice Shelf with tidally induced vertical mixing. *Antarc. Sci.,* **2,** 29–42.

Steele, M., G. L. Mellor, and M. G. McPhee, 1989: Role of the molecular sublayer in the melting or freezing of sea ice. *J. Phys. Oceanogr.,* **19,** 139–147.

Tennekes, H., and J. L. Lumley, 1972: *A First Course in Turbulence.* The MIT Press, 300 pp.

Toggweiler, J. R., and B. Samuels, 1995: Effect of sea ice on the salinity of Antarctic bottom waters. *J. Phys. Oceanogr.,* **25,** 1980–1997.

Wexler, H., 1960: Heating and melting of floating ice shelves. *J. Glaciol.,* **3,** 626–645.

Williams, M. J. M., R. C. Warner, and W. F. Budd, 1998: The effect of ocean warming on melting and ocean circulation under the Amery Ice Shelf, East Antarctica. *Ann. Glaciol.,* **27,** 75–80.

——, A. Jenkins, and J. Determan, 1999: Physical controls on ocean circulation beneath ice shelves revealed by numerical models. *Ocean, Ice, and Atmosphere Interactions at the Continental Margin,* S. S. Jacobs and R. Weiss, Eds., *Antarctic Res. Ser.,* Amer. Geophys. Union, 285–300.